An experimental study of the bond behavior of twisted steel bars embedded in mortar cylinders and in the joints of masonry wallettes

(Article begins on next page)

23 April 2024

AN EXPERIMENTAL STUDY OF THE BOND BEHAVIOR OF TWISTED STEEL BARS EMBEDDED IN MORTAR CYLINDERS AND IN THE JOINTS OF MASONRY WALLETTES

Cristina Gentilini[1a*], Francesco Finelli[2b], and Christian Carloni[3c]

[1]Department of Architecture – DA, University of Bologna, Viale del Risorgimento 2, 40136 Bologna, Italy

[2]Department of Civil, Chemical, Environmental and Materials Engineering – DICAM, University of Bologna, Viale del Risorgimento 2, 40136 Bologna, Italy

[3]Department of Civil and Environmental Engineering, Case Western Reserve University, 10900 Euclid Ave, Cleveland (OH), 44106, U.S.A.

[a]cristina.gentilini@unibo.it, [b]f.finelli@namirial.com, [c]christian.carloni@case.edu

*corresponding author

Highlights

- Pull-out tests of steel bars inserted in mortar cylinders were conducted

- Pull-out tests of steel bars inserted in masonry wallettes were conducted

- Different bonded lengths were considered

- Bar rotation during extraction was observed

Keywords: bond behavior, near-surface mounted technique, twisted steel bar, pull-out test, mortar cylinders, masonry wallettes.

ABSTRACT

Among the different strengthening techniques available to reinforce masonry buildings, the near-surface mounted technique consists in inserting reinforcing elements of high-strength material in grooves realized by removing part of the mortar in the horizontal bed joints of a masonry wall. The present study deals with two experimental campaigns on pull-out tests conducted on twisted steel bars embedded concentrically in mortar cylinders and in the mortar bed joints of masonry wallettes as in *in-situ* applications. In order to compare the results between cylindrical and masonry specimens, the same bonded lengths are considered.

1

1. INTRODUCTION

The main structural deficiencies of masonry buildings are related to the almost-inexistent tensile strength, as the bond strength between mortar and fired-clay brick is very low, and the limited effectiveness of the connections between the masonry elements [1, 2]. Thus, masonry buildings are susceptible to seismic actions [3], as unfortunately highlighted in the recent Italian events of L'Aquila in 2009, Emilia Romagna in 2012, and Amatrice in 2016 [4-8]. When fair-faced masonry buildings necessitate retrofitting, reinforced structural repointing may be a feasible solution since it does not violate the aesthetic requirements of a historical building since the reinforcement is embedded in the joints [9-13]. The strengthening elements can be of different shapes and materials. Fiber-reinforced polymer (FRP) thin strips or bars made of carbon (CFRP), AR glass, or basalt fibers embedded in an organic matrix are typically used, although stainless steel bars have been studied as well and will be the focus of this paper. Structural repointing is also known as near-surface mounted (NSM) technique, since the reinforcing material is inserted into 10-20 mm-deep grooves usually carved in the mortar bed joints by means of a circular saw. The reinforcing elements are embedded in the joint grooves by means of an organic material such as epoxy (typically thermosetting), cementitious mortars modified with the addition of organic additives, or cementitious-based mortars or lime-based mortars. When possible, the reinforcing elements are applied on both sides of the wall, and in some cases, they are connected by ties placed transversely in the wall [14].

The use of repointing for masonry structures is fairly common. However, only few studies in the literature have focused on the bond performance of NSM reinforcement embedded in masonry [15-20]. The most important contributions dealing with pull-out tests of structural repointing can be roughly divided into two main groups of researchers. In the United States, most studies investigated the bond performance of carbon or glass FRP bars embedded in the bed joints of masonry specimens made of concrete blocks [21, 22]. The variables that have been considered are the bonded length, bar diameter, groove size with respect to the bar diameter, embedding material (epoxy or latex modified cementitious mortar), as well as the bar surface condition. The second major group of studies have been conducted in Australia and New Zealand and dealt with pull-out tests of CFRP strips embedded with epoxy resin in masonry specimens made of solid fired-clay bricks [16, 23-25]. In these experimental campaigns, several parameters were taken into account: the strip

bonded length, the direction (parallel or orthogonal) of the reinforcing elements with respect to the direction of the bed joints, the effect of cyclic loadings, as well as the size of the strips. It should be noted that in this group of experimental campaigns the NSM CFRP strips were inserted into grooves cut through the fired-clay bricks rather than placed where the mortar joints were located.

Starting from the available experimental results on pull-out tests, simple analytical models have been developed to predict the bond properties such as bond capacity, effective bond length, and shear stress-slip relationship for concrete or fired-clay brick masonry substrates that are useful to predict the performance of structures that are reinforced with NSM bars or strips [26, 27].

To the best of the authors' knowledge, none of the aforementioned works are related to study the bond behavior of NSM steel bars embedded in the bed joints of fired-clay brick masonry, employing as groove-filling material an inorganic matrix such as a structural mortar. To fill this gap, the aim of this work is to present the results of two extensive experimental campaigns that focus on the bond behavior of spiral-shaped stainless-steel bars. In the first campaign, in order to get a preliminary insight on the bond behavior of these bars, a series of pull-out tests are conducted on steel bars concentrically embedded in cylinders made of the same structural mortar used to embed the bars in the masonry grooves. The bars made of ultra-high strength steel are characterized by a helical shape. Several bonded lengths are considered. In the second experimental campaign, the same type of bars is inserted with the same structural mortar in the horizontal bed joints of masonry wallettes in order to reproduce more closely the *in-situ* application. The same bonded lengths investigated in the first experimental campaign are considered in the second set of tests for comparison.

2. EXPERIMENTAL PROGRAM

2.1. Materials: mortars and bricks

Two different types of mortar were employed to construct the specimens: 1) a mortar used for structural applications herein used to cast the cylinders of the first campaign and embed the bars inside the masonry specimens of the second campaign (hereinafter referred to as mortar_s), and 2) a low-strength mortar herein employed for the masonry joints in the second campaign (hereinafter referred to as mortar_j).

3

Mortar_s was a commercially-available ready-mix mortar, M15 class according to EN 998-2 [28], which was comprised of natural hydraulic lime and siliceous sand. From each batch of mortar employed to cast the cylinders of the first campaign, six prisms (nominal dimensions $40 \times 40 \times 160$ mm^3) were cast and left to cure for two months under a plastic sheet in the laboratory at room conditions. It should be noted that the curing period was longer than the conventional 28 days, because the mortars employed for the construction of the specimens employed in the experimental campaign (both cylinders and wallettes) contained a fraction of natural hydraulic lime. According to the authors' experience, this period of time allowed to achieve a satisfactory hardening of the selected mortars [29]. According to EN 1015-11 [30], three prisms were tested to determine compressive, f_c, and flexural, f_f, strengths. In order to determine the elastic modulus, E, two strain gauges were applied symmetrically on two lateral surfaces of the remaining mortar prisms and tested according to EN 12390-13 [31] as shown in Figure 1a. In Figure 1b, the compressive stress-strain curves of the mortar_s prisms used to determine the elastic modulus from one batch are reported. The average compressive and flexural strengths and elastic modulus of mortar_s for all batches resulted equal to 16.2 MPa (CoV=3.7%), 3.8 MPa (CoV=6.9%), and 10.5 GPa (CoV=8.2%), respectively. The mechanical properties were determined when the pull-out tests were started.

Mortar_j employed for the joints of the masonry specimens was a ready-mix commercially-available mortar, M5 class according to EN 998-2 [28], which was comprised of natural hydraulic lime, siliceous sand, and dolomitic limestone. From each batch of mortar used to construct the joints of the masonry specimens, six mortar prisms (nominal dimensions $40 \times 40 \times 160$ mm^3) were cast and cured as the mortar_s prisms. They were tested according to EN 1015–11 [30] to obtain the mechanical properties. The average compressive and flexural strengths of mortar_j for all batches, tested when pull-out tests were performed, were equal to 12.7 MPa (CoV=5.3%) and 2.8 MPa (CoV=4.8%), respectively.

Solid fired-clay bricks (nominal dimensions $250 \times 120 \times 55$ mm^3) were employed to construct the masonry wallettes. The compressive strength of the bricks was evaluated according to EN 772–1 [32] and resulted equal to 16.9 MPa (CoV=2.5%).

4
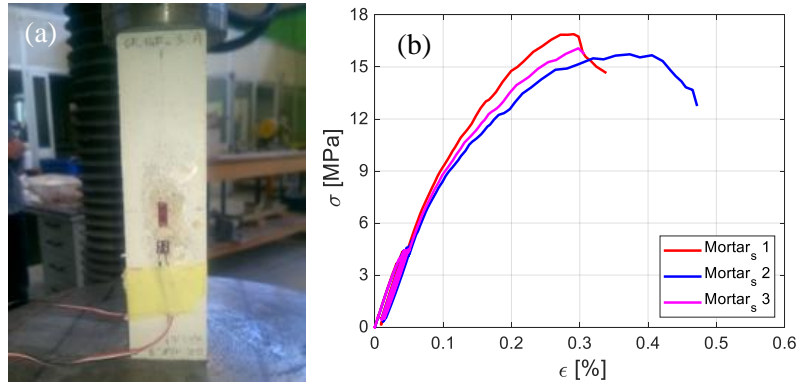
Figure 1. Mechanical characterization of mortar_s: (a) compression test to determine the elastic modulus, and (b) stress-strain curves.

2.2. Materials: twisted steel bars

The bars used for repointing were made of high-strength steel (AISI 316) and had a helical shape to improve adhesion (Figure 2a). The bars were formed from a circular steel wire, which was cold worked to obtain the cross-sectional shape shown in Figure 2b. Afterwards, the bars were twisted while applying a tension force to reach the final helical shape. Nominal diameter, ϕ, and cross-sectional area, A, were equal to 6 mm and 8 mm^2, respectively. Steel bars were tested to determine Young's modulus, E, and tensile strength, f_t.

(d)

bi-component epoxy resin

twisted steel bar

plastic cap
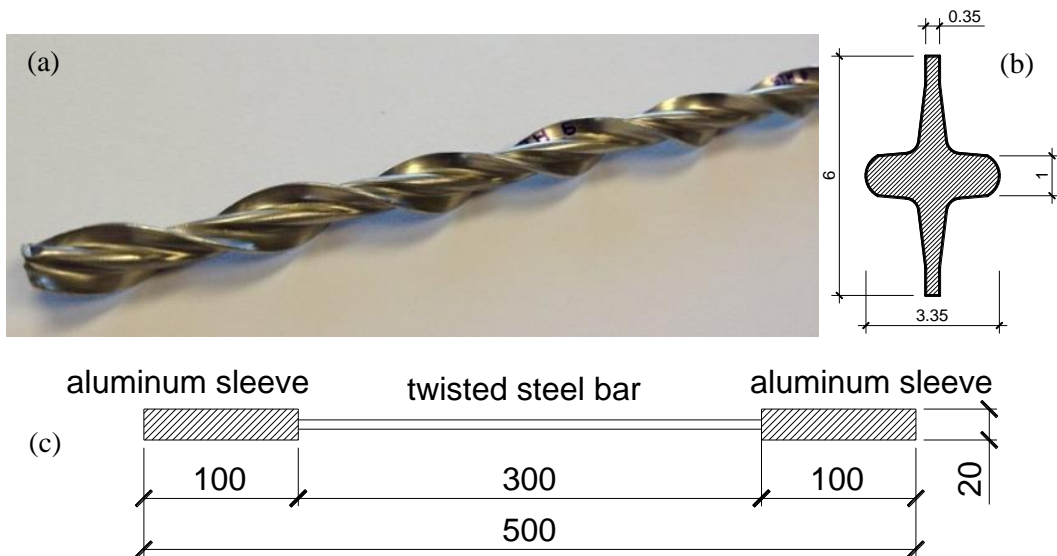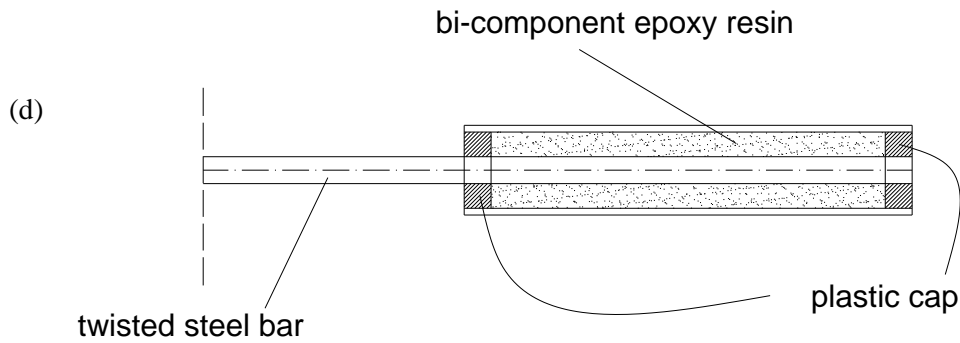
Figure 2. a) Photo of the twisted steel bar, b) cross-section of the helical-shape bar, c) specimen dimensions for the tensile test, and d) detail of the anchoring system for the tensile test. (Dimensions in mm).

Preliminary tests indicated that direct gripping of the helical bars would have damaged the bars and compromised the tension test results. Thus, to avoid undesired failure modes of the bars tested in tension, aluminum hollow cylinders were epoxy-glued at each end of the bars. The length of the cylinders (or sleeves) were determined through preliminary tests, and it was found that a length of 100 mm was sufficient to run the tension tests of the bars up to failure (Figure 2c). The bars were inserted into the sleeves, which were filled with a thixotropic bi-component epoxy resin and left to cure for at least 24 hours. The bars were placed concentrically in the pipes, plastic caps with a hole to insert the bar were applied at both end of each sleeve (Figure 2d). The total length of the bars was 500 mm, with a free length of 300 mm. A 100 kN universal testing machine was used for the tests and the load was applied at a constant stroke rate of 2 mm/min until failure of the specimen occurred. Three specimens, out of eleven bars tested, were equipped with a 100 mm-gauge length extensometer placed in the central portion of the bar to measure the elongation and determine Young's modulus (Figure 3a). To check if the gripping system (aluminum cylinders) could affect the test results, the location along the bar where rupture occurred was observed and reported (Figure 3b). The average tensile strength resulted equal to 1226 MPa (CoV=2%), while the average elastic modulus based on three tests was equal to 143 GPa (CoV=7%). Figure 3c shows the stress-strain curves for the three bars equipped with extensometer. After an initial linear-elastic branch, the bars exhibited a nonlinear behaviour followed by an almost-horizontal branch until tensile failure occurred.
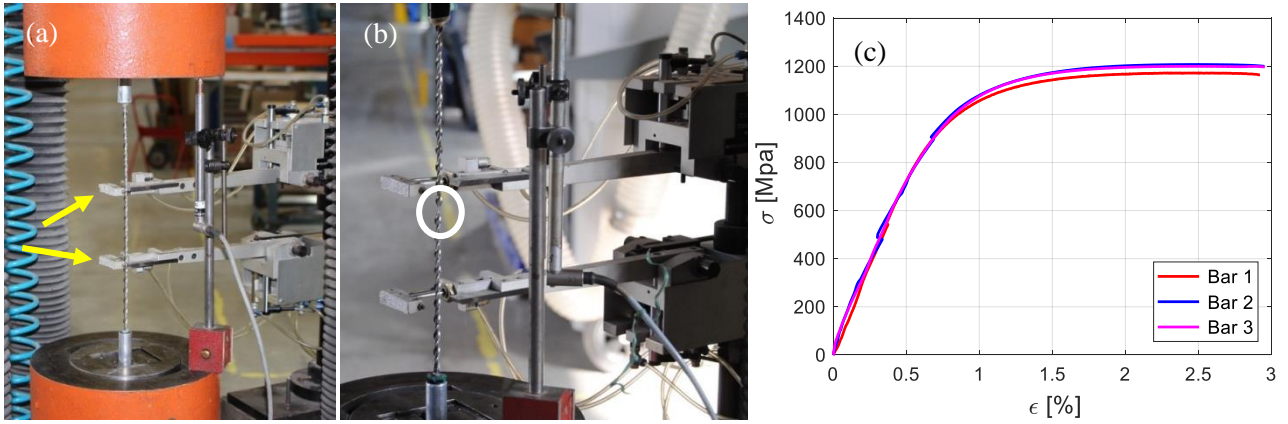
6

Figure 3. Mechanical characterization of twisted (helical shaped) steel bars: a) bar at the beginning of the tensile test (the extensometer employed to measure the bar length variation is indicated with yellow arrows), b) bar at the end (failure) of the test, and c) stress-strain curves.

2.3. Cylindrical specimens

Mortar cylinders of nominal diameter equal to 150 mm were cast with mortar_s and twisted steel bars of different lengths were embedded concentrically. PVC tubes were used as molds (Figure 4a). A length of 50 mm from the top of the cylinder was left unbonded, such that during the pull-out, failure was given to the bar pull-out and not to an incorrect tensile failure of the mortar cylinder [33, 34]. Plastic pipes were used to create the bond break (Figure 4b) and in order to avoid the formation of voids, the compaction of the fresh mortar was carried out manually with a rod (Figure 4c). The bonded length of the bar is named L_B in the remainder of the paper. The bar extended 300 mm and 100 mm from the top and bottom ends of the cylinders, respectively. Cylindrical specimens with different bonded lengths L_B, namely 150, 250, 350, 450, and 700 mm, were cast. The total height of those cylinders was 50 mm longer than the corresponding bonded length because of the additional unbonded length. Three specimens for each bonded length were constructed, which correspond to 15 cylinders in total (Figure 4d). Specimens were cured in laboratory conditions for two months under a polyethylene sheet. At the end of the two months, prior to testing an aluminum sleeve was installed at the end of the bar to improve gripping by the machine jaws. The sleeves were the same as the ones used in the direct tensile tests. They were 100 mm long, 2 mm thick, and were filled with epoxy. Specimens were named C-X-Z, were C stands for cylindrical, X is the bonded length L_B, and Z is the specimen number. A sketch of the geometry of cylindrical specimens C-L_B with a generic bonded length L_B is shown in Figure 5.

7

Figure 4. Construction phases of the cylindrical specimens: a) and b) the bar is positioned concentrically in the cylinder mold, a plastic tube is used to create a bond break of length equal to 50 mm from the top face of cylinder, c) mortar_s is manually rodded in order to avoid the formation of large voids, and d) the cylinders are left to cure in lab conditions.
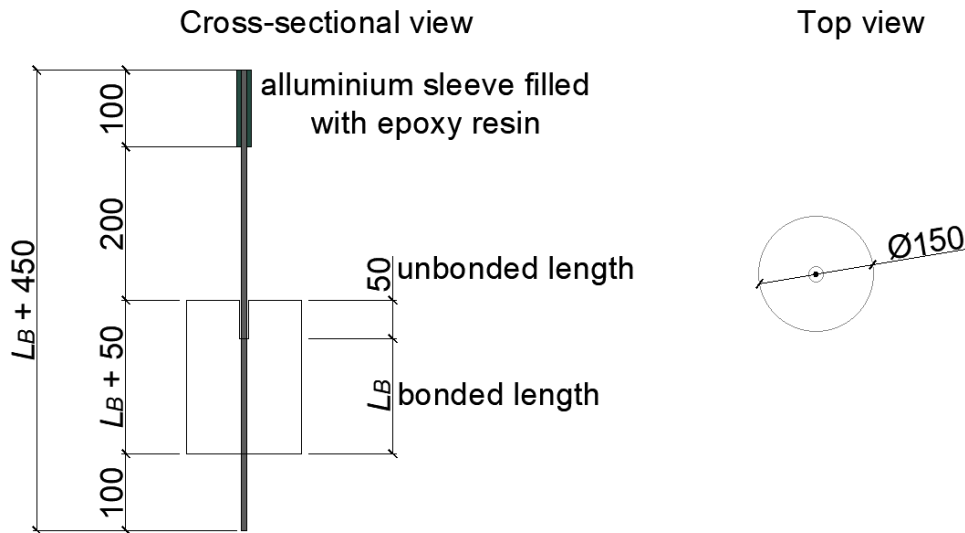
Figure 5. Sketch of a cylinder with a bar embedded for a length L_B: on the left, longitudinal section and on the right, top view. (Dimensions in mm).

2.4. Masonry specimens

The masonry specimens were wallettes, characterized by a single wythe (depth 120 mm), four regular courses and 10 mm-thick mortar joints (made of mortar_j). As stated in previous sections, in the repointing technique applied to an existing masonry building, the strengthening material is usually inserted in grooves realized by means of a circular saw along the horizontal bed joints. In this experimental campaign, the twisted bars were inserted during the construction phase, given the small size of the specimens, since cutting the grooves with a saw would have damaged the specimens themselves. In order to embed the bars in the central bed joint, the two external sides of the joint were kept free from the mortar by inserting two wooden slats (10 mm thick and 22 mm wide) as shown in Figure 6a and 6b. The remaining joints were completely filled with mortar_j (Figure 6c). After one week of curing, the wooden slats were removed, which left two grooves in the specimens (Figure 6d). The outer surface of the specimens and the grooves were manually wet with a sprayer (Figure 6d), prior to injecting the first layer of the structural mortar (mortar_s) as shown in Figure 6e. Once the mortar filled the groove, the bar was pressed inside the groove so that the bar centroid was approximately at 18 mm from the outer surface of the specimen. A second layer of mortar_s was employed to seal the joint (Figure 6f). It should be noted that two different mortars, one to realize the joints and the other, called 'structural' to embed the strengthening bars, were employed to build the wallettes in order to mimic the in-situ conditions and to

9

represent as close as possible a situation than can be found on a real application. In fact, in real applications, usually the mortar of the joints is of scarce quality both in terms of mechanical and physical properties, while the mortar that is employed to embed the strengthening material has enhanced structural characteristics. In general, the different deformation properties between the two mortars could affect the performance of the reinforcement, thus in order to increase the compatibility level between new and original materials, the chosen mortar_s contained a fraction of natural hydraulic lime, resulting in a less rigid and a more porous material with respect to an only cement-based mortar, which is usually employed for concrete reinforcement.

In the wallettes, only the central portion of the bars was bonded to the masonry specimens, while the end regions were left unbonded. In particular, an unbonded length equal to 50 mm was left from the top surface of the specimen at the loaded end, while on the bottom side, the unbonded length varied with the size of the specimens. In fact, the length of the specimens changed with the bonded length of the bar. Except for the 150 mm embedded length, for longer lengths, more than one brick was laid horizontally alternated by head joints. In detail, the wallettes with an embedded bar of 150, 250, 350, 450 and 550 mm had a total nominal length equal to 250, 410, 510, 510 and 640 mm, respectively. For all wallettes, the bars extended from the top and bottom surfaces of the specimens by 300 mm and by 100 mm, respectively. It should be noted that for each specimen, two bars (labelled bars A and B in the remainder of the paper) were inserted symmetrically on the opposite lateral surfaces of the wallettes along the central joint. One bar at the time was tested and it was assumed that the presence of one bar did not to influence the other during their test, since the distance between them was approximately 75 mm. To confirm this assertion, additional considerations are given in Sections 3.2 and 5. Different bonded lengths of the bars were considered and four masonry specimens were built for each bonded length, thus a total of 8 masonry specimens had the bars embedded with the same bonded length L_B. In order to make a comparison with the bond behavior of the bars embedded in the cylinders, the same bonded lengths were considered. However, masonry specimens with bars embedded for a length of 700 mm were not constructed due to limitations in the clearance height of the testing machine. An additional bonded length equal to 550 mm for masonry specimens was considered as a substitute of the 700 mm bonded length of the cylinders. Masonry specimens were cured for two months in laboratory conditions under a polyethylene sheet to facilitate the hydration of the binder, and after the curing period and prior to testing, a sleeve filled with epoxy was

installed at the end of each bar. Masonry specimens were named W-X-ZY, were W stands for masonry wallette, X is the bonded length L_B, Z is the specimen number, and Y stands for A or B depending on which of the two bars inserted in the specimen was tested. Figure 7 shows a sketch of a masonry specimen (W-L_B) with two bars bonded for a length L_B in the central bed joint.
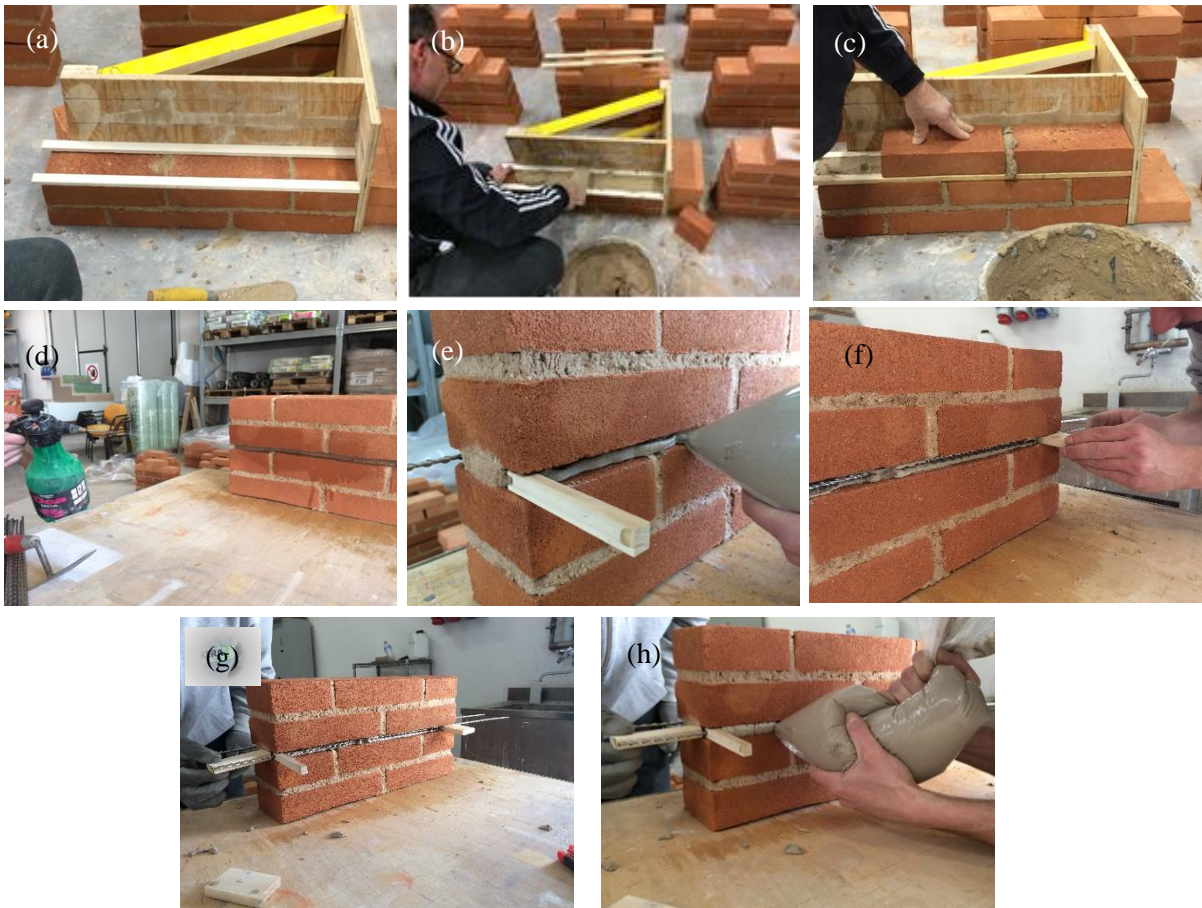
Figure 6. Construction phases of the masonry wallette with $L_B = 450$ mm: a) in the second layer two wooden slats placed symmetrically were used to create a groove, b) casting of the central mortar joint, c) bricks were placed on top of the central joint, d) after 7 days of curing, wooden slats were removed and the grooves were wet, e) the grooves were partially filled with a first layer of mortar_s, f) bar was pushed in the fresh mortar in order it was completely surrounded by mortar_s, g) insertion of wooden elements for correct bar positioning and f) a final layer of mortar_s was used to seal the grooves.
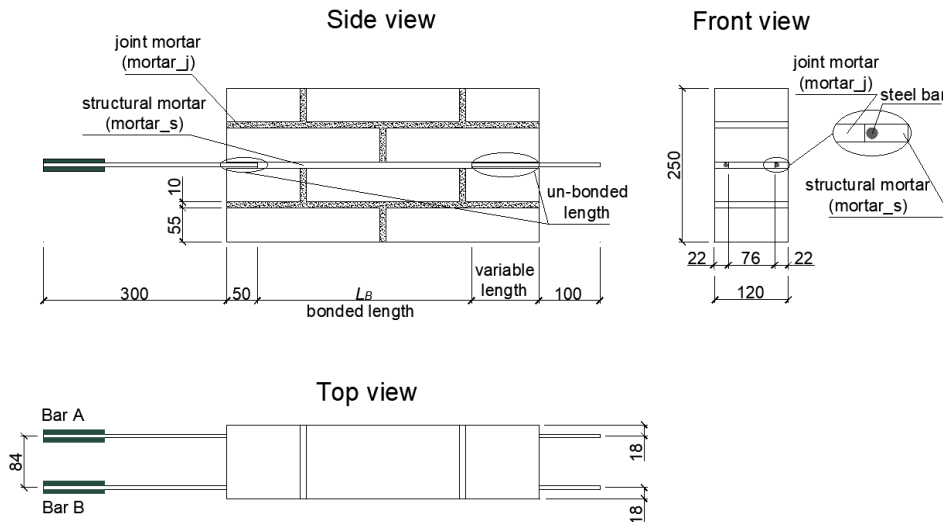
Figure 7. Sketch of a masonry wallette with two bars embedded for a length L_B in central bed joint. (Dimensions in mm).

2.5. Pull-out test: cylindrical and masonry specimens

Tests were conducted using a 100 kN servo-hydraulic testing machine. Figures 8a and 8b show the sketch and photo, respectively, of the experimental set-up used for the cylindrical specimens. A steel plate (bottom steel plate in Figure 8a) was gripped by the bottom head of the machine through a stud bolted to the plate. The specimen was placed on the bottom plate using spacers since the bar was extending beyond the cylinder base. A steel plate, with an 80 mm-diameter central hole (top steel plate in Figure 8a), was placed on the top of the specimen and the two plates (top and bottom) were connected by means of four threaded rods. The helical bar was gripped by the top machine head through the aluminum sleeve. It should be noted that prior to placing the cylindrical specimen on the testing fixture, a rapid set self-levelling mortar was applied on the top surface of the cylinder in order to smoothen out the surface that was in contact with the restraining top steel plate and ensure an even distribution of the load. To measure the relative displacement between the bar and the cylinder, two linear differential displacement transformers (LVDTs) with a stroke equal to 20 mm were mounted on the top plate using magnets. These two LVDTs are named $LVDT_{1,top}$ and $LVDT_{2,top}$ in the remainder of the paper. They reacted off of an aluminum circular plate that was attached to the bar in the portion of it just above the top plate (Figure 8c). It should be noted that a circular plate was used since the helical bar rotated about its longitudinal axis as it was pulled out. The displacements measured by $LVDT_{1,top}$ and $LVDT_{2,top}$ are named s_{l1} and s_{l2}, respectively, while the average of the two measurements is defined as the bar slip at the loaded-end, s_l,

12

in this paper. It should be noted that in the slip definition, the elastic deformation of the bar between the point where the LVDTs were placed and the beginning of the bonded area was considered [35]. Once the bar was clamped by the jaws, the spacers at the bottom were removed. Two LVDTs (stroke equal to 10 mm) named $LVDT_{1,bottom}$ and $LVDT_{2,bottom}$ were used to measure the relative displacement between the free-end of the bar and the base of the cylinder. The LVDT holders were screwed into the bottom lateral surface of the cylinder (Figure 8d). The LVDTs reacted off of an aluminum circular plate attached to the free end of the bar in the portion extending beyond the cylinder (Figure 8d). The displacements measured by $LVDT_{1,bottom}$ and $LVDT_{2,bottom}$ are named s_{f1} and s_{f2}, respectively, while the average of the two measurements is defined as the bar slip at the free-end, s_f, in this paper. All the tests were conducted in displacement control mode using the machine stroke. For the first part of the test until the peak load was attained, the stroke rate was equal to 5 μm/s. After the peak load was reached, the rate was increased to 0.05 mm/s until the end of the test.

A similar set-up was used for the masonry specimens, as shown in Figures 9a and 9b. As for the cylinders, two LVDTs were mounted on the top plate (namely $LVDT_{1,top}$ and $LVDT_{2,top}$) to measure the relative displacement between the bar loaded end and the masonry wallette (Figure 9c). It should be noted that for the masonry specimens the spacers at the bottom were replaced by an intermediate steel plate that supported the masonry wallette and had a central hole to let the bar at the bottom of the specimen extends through the plate itself. In addition, since for each masonry wallette, two bars were inserted in the mortar joints (one on each opposite longitudinal face of the wallette), when one of the bars was tested the masonry wallettes resulted eccentrically placed with respect to the center of the top plate (Figure 9d). Cardboard was used in between the top plate and the surface of masonry to avoid any stress concentration. Due to the eccentric placement of the masonry wallette with respect to the top plate, only one LVDT, named $LVDT_{bottom}$ (Figure 9e), was used at the bottom of the specimen to measure the bar slip at the free-end, s_f. $LVDT_{bottom}$ reacted off of an aluminum circular plate that was attached to the free end of the bar. Pull-out tests on masonry specimens were conducted under displacement control using the same rates as the cylindrical specimens. It should be noted that during the tests both for cylinders and masonry specimens, the top machine head was left free to rotate.

Figure 8. Pull-out test set-up for cylindrical mortar specimens: (a) sketch, (b) photo of representative specimen, (c) photo of $LVDT_{1,top}$ and $LVDT_{2,top}$ used to measure the loaded-end slip, and (d) photo of $LVDT_{1,bottom}$ and $LVDT_{2,bottom}$ used to measure the free-end slip (the arrows indicate the LVDT holders).
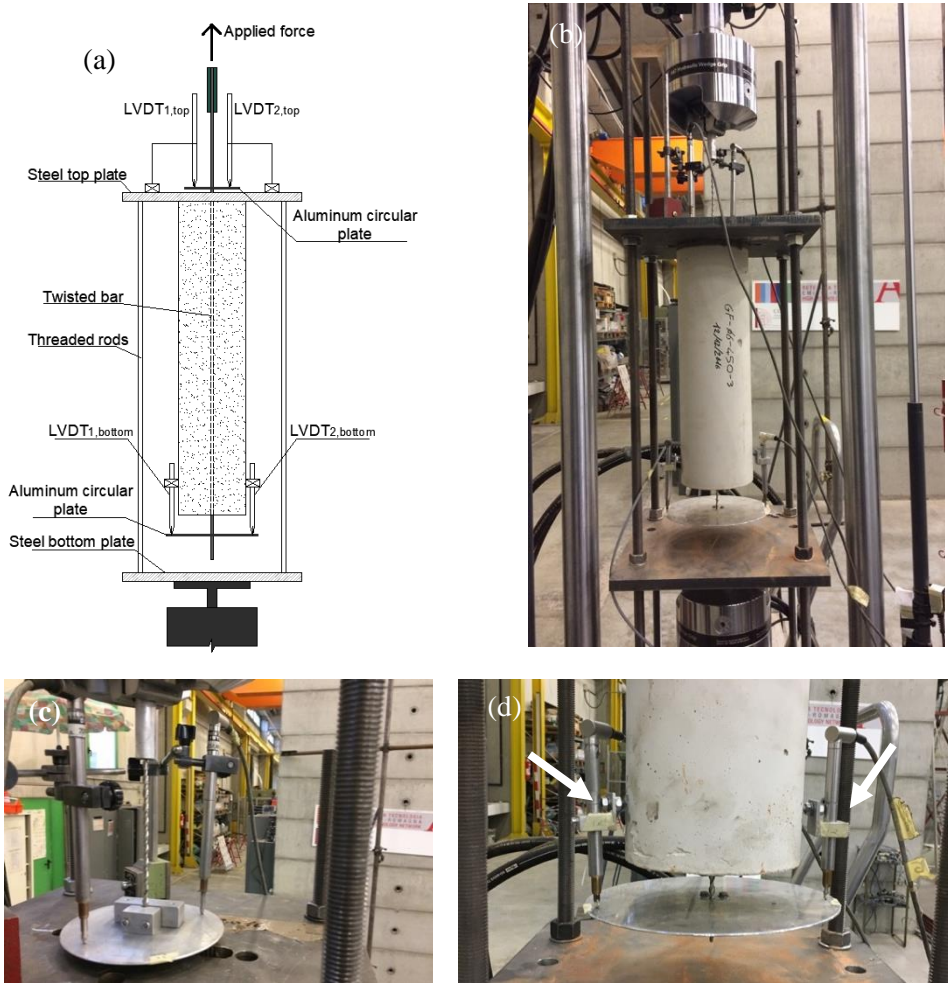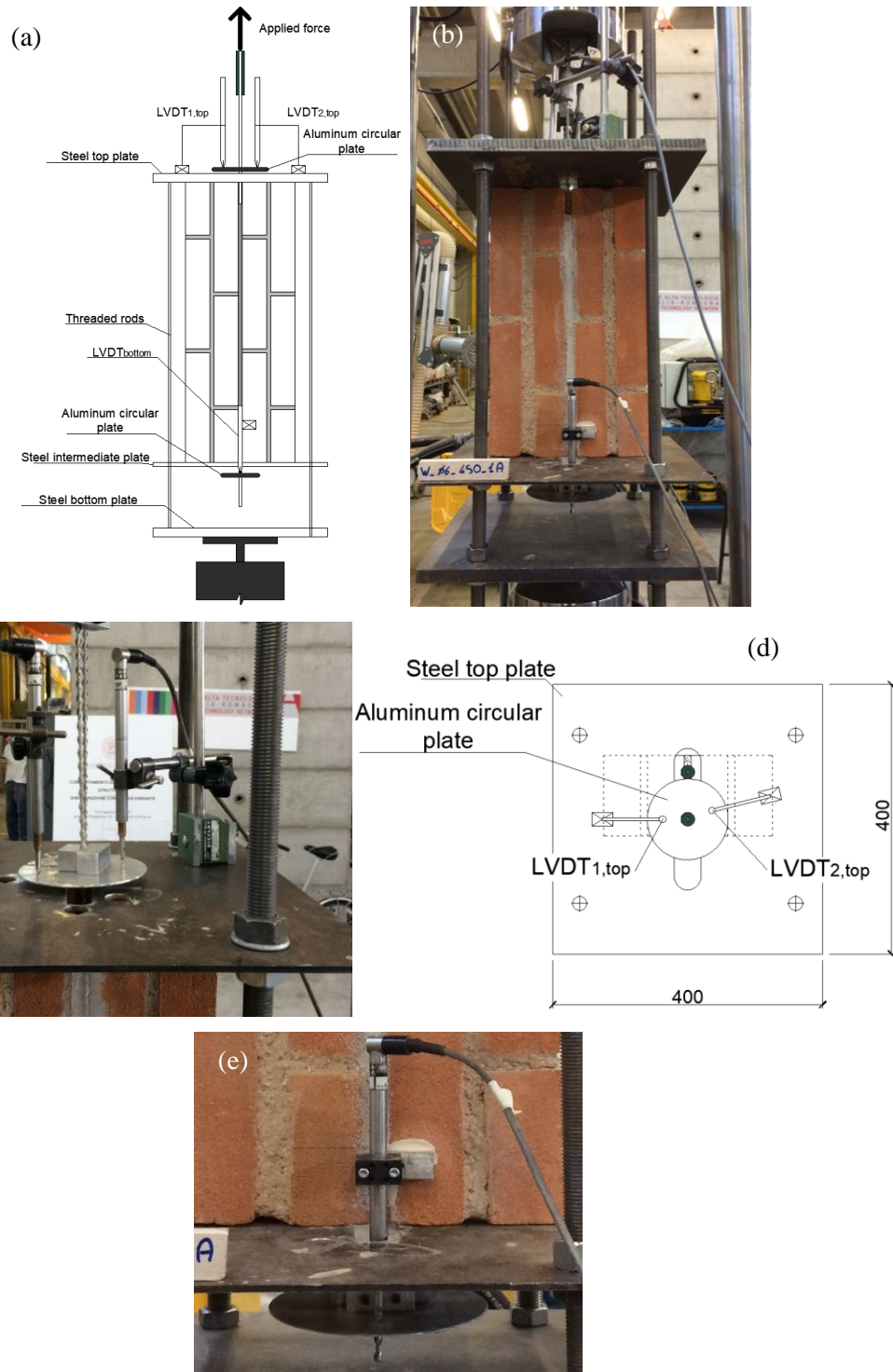
Figure 9. Pull-out test set-up for masonry specimens: (a) sketch, (b) photo of representative specimen, (c) photo of $LVDT_{1,top}$ and $LVDT_{2,top}$ to measure the loaded-end slip, (d) sketch of the top plate, and (e) photo of $LVDT_{bottom}$ used to measure the bar free-end slip. (Dimensions in mm).

3. RESULTS OF THE PULL-OUT TESTS FOR THE CYLINDRICAL SPECIMENS

In this section, the results of 15 pull-out tests conducted on the cylindrical specimens are presented. Bars slipped out of the cylinders until the test was stopped because the maximum LVDT stroke was reached (Figure 10), except for cylinders with L_B = 700 mm for which bar rupture occurred. It should be noted that both top and bottom LVDTs were removed close to the attainment of their maximum stroke, and then the test was resumed until the machine stroke was close to its maximum. In Figures 11a and 11b, the applied load (F) versus loaded-end slip (s_l) and the applied load versus free-end slip (s_f) responses of a representative cylindrical specimen with bonded length L_B = 150 mm are plotted, respectively. In both Figures 11a and 11b, the applied load versus each LVDT readings curves are also reported together with their averages. It can be observed that the curves of each LVDT are very similar and overlapping with the average, which indicates that the bar was pulled out without any significant bending. In Figure 11c, the two average curves F-s_l and F-s_f are compared.
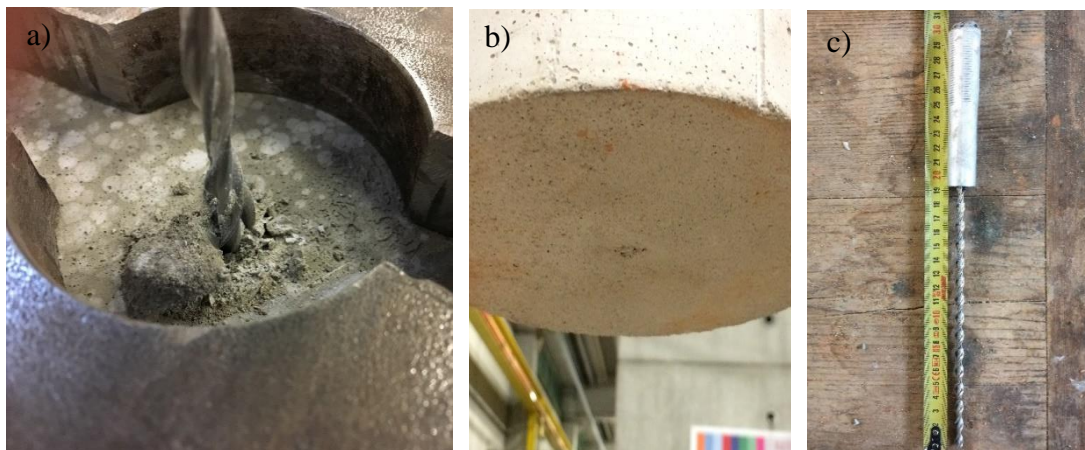
Figure 10. (a) Top; (b) bottom view of a representative cylindrical specimen at the end of the test; c) tensile rupture of the bar that attained for cylinders with L_B = 700 mm.

Referring to Figure 11c, three main branches can be distinguished in the $F - s_l$ curve: 1) an initial pseudo-linear portion for low load values followed by a non-linear branch until the peak load F_m is reached; 2) a load drop branch; and 3) an ascending almost-linear branch until the end of the test. In the first branch, the free-end slip is different from zero, although the values are very small, for the majority of the branch, as shown in the call-out (Figure 11d). In the third branch, the free-end slip increases almost linearly like s_l but with a lower rate.

16

During the pull-out test, due to its twisted shape, the bar was subjected to a combined action of tension and torsion. In fact, while elongating and slipping, the bar rotated about its longitudinal axis from the beginning of the test. It should be noted that the bar rotation could not be measured during the experimental tests, but it was easily observable by means of the rotation of the circular plates that were rigidly connected to the bar, see Figures 8c and 8d. Thus, even small bar rotations that occurred at the beginning of the test were made more visible by the plate rotation. After the load drop, visual observation during the test suggested that the bar rotation rate increased. At the end of the test, the bar rotation was partially released and a rotation in the opposite direction was observed as the bar was unloaded. This behavior was already pointed out also in another experimental campaign, where bars with the same cross-sectional shape were pulled out from bricks made of different materials in a similar test set-up [20].

Due to the good agreement between the readings of the two LVDTs at the top as well as between the two at the bottom for all specimens, only the average curves are shown in Figure 12. Figures 12a, 12b, 12c, 12d, 12e collect the curves obtained from the pull-out tests for the cylinder groups: C-150, C-250, C-350, C-450 and C-700, respectively. All the responses are characterized by a similar shape, and the three branches as described above can be observed for all specimens, except for specimens with L_B = 700 mm, (Figure 12e), which are characterized by an initial pseudo-linear portion for low load values followed by a non-linear branch, since the bars failed due to rupture close to the cylinder top surface. It should be noted that in the case of bars with $L_B \leq 450$ mm (Figure 12a-12d), the slip at the free end is almost zero before the peak load is attained, while once the peak load is reached the free end slip increases significantly. Slips at the free end prior to the attainment of the peak load are zero for L_B = 700 mm. Analyzing the load-slip curves for all the specimens, the influence of the bonded length can be studied. The pull-out peak load F_m increases as the bonded length increases and, correspondingly, also the slip at the loaded end at peak, s_{ml}, increases, as reported in the literature [19]. Further, it can be noted that as the bonded length increases, the non-linearity of the first branch of the F - s_l curves close to the peak load becomes more pronounced. In general, a good agreement among the curves for the specimens with the same bonded length is observed, which indicates repeatability and reliability of the tests. No splitting failure of the cylinders was observed in any specimen.

17

The results of the pull-out for all cylindrical specimens are collected in Table 1. In particular, the peak load F_m for each specimen and the average value $\bar{F}_m$, for each group are listed. It should be noted that for peak load F_m is intended the load value registered at the end of the first branch, which cannot correspond to the maximum absolute load value of the curve, since in the last ascending branch higher load values than the first peak were attained in some specimens. The corresponding slips at the loaded-end s_{ml} and average value, $\bar{s}_{ml}$ for each group are reported as well. It can be noted that results for each group are consistent and characterized by a low coefficient of variation (CoV). Only cylinders C-450 show a higher CoV compared to the others, due to the experimental outcomes of specimen C-450-2, which showed a lower peak load and slip at the loaded end with respect to specimens of the same group. However, results for this specimen are consistent, since the load value is smaller, but correspondingly also the s_{ml} value is lower. Possible reasons of such different results may be related to manufacturing issues (curing conditions) and/or a possible misalignment of the bar.

The load drop ΔF for each specimen, calculated as the difference between the first peak load value (F_m) and the load value at the end of the load drop branch, with the corresponding average value $\Delta \bar{F}$ for each group are reported in Table 1.
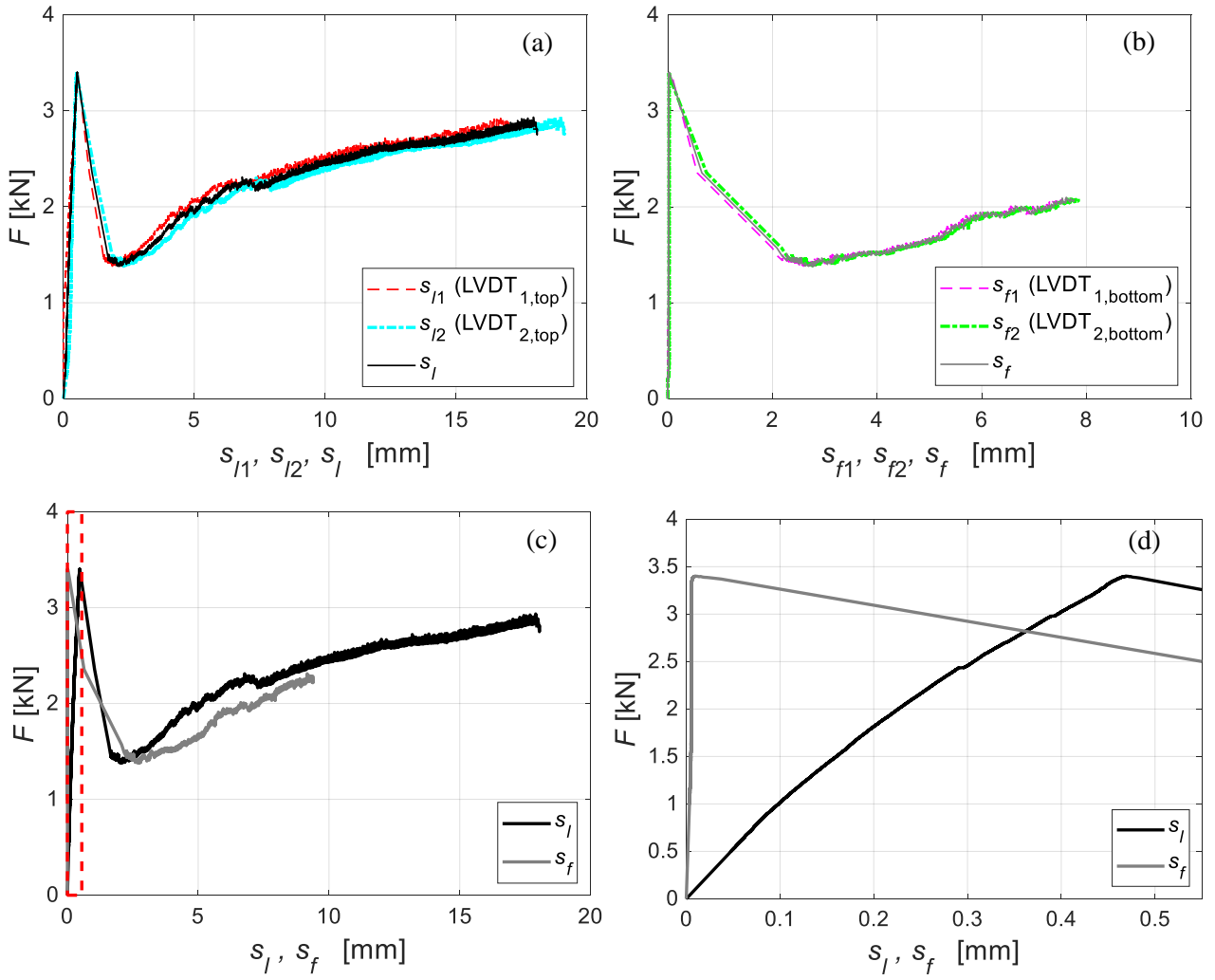
Figure 11. Load-slip curves of a representative cylindrical specimen (C-150-1, L_B = 150 mm): (a) $F - s_l$, $F - s_{l1}$ and $F - s_{l2}$ curves, (b) $F - s_f$, $F - s_{f1}$ and $F - s_{f2}$ curves, (c) $F - s_l$ and $F - s_f$ curves and (d) call-out of the $F - s_l$ and $F - s_f$ curves at the beginning of the test.

Figure 12. F - s_l and F - s_f curves for cylindrical specimens. In each row, curves for specimens with the same bonded length are collected: a) C-150; b) C-250; c) C-350; d) C-450 and e) C-700.

20

Table 1. Pull-out test results for cylindrical specimens (coefficient of variation, CoV, in percentage within parentheses).

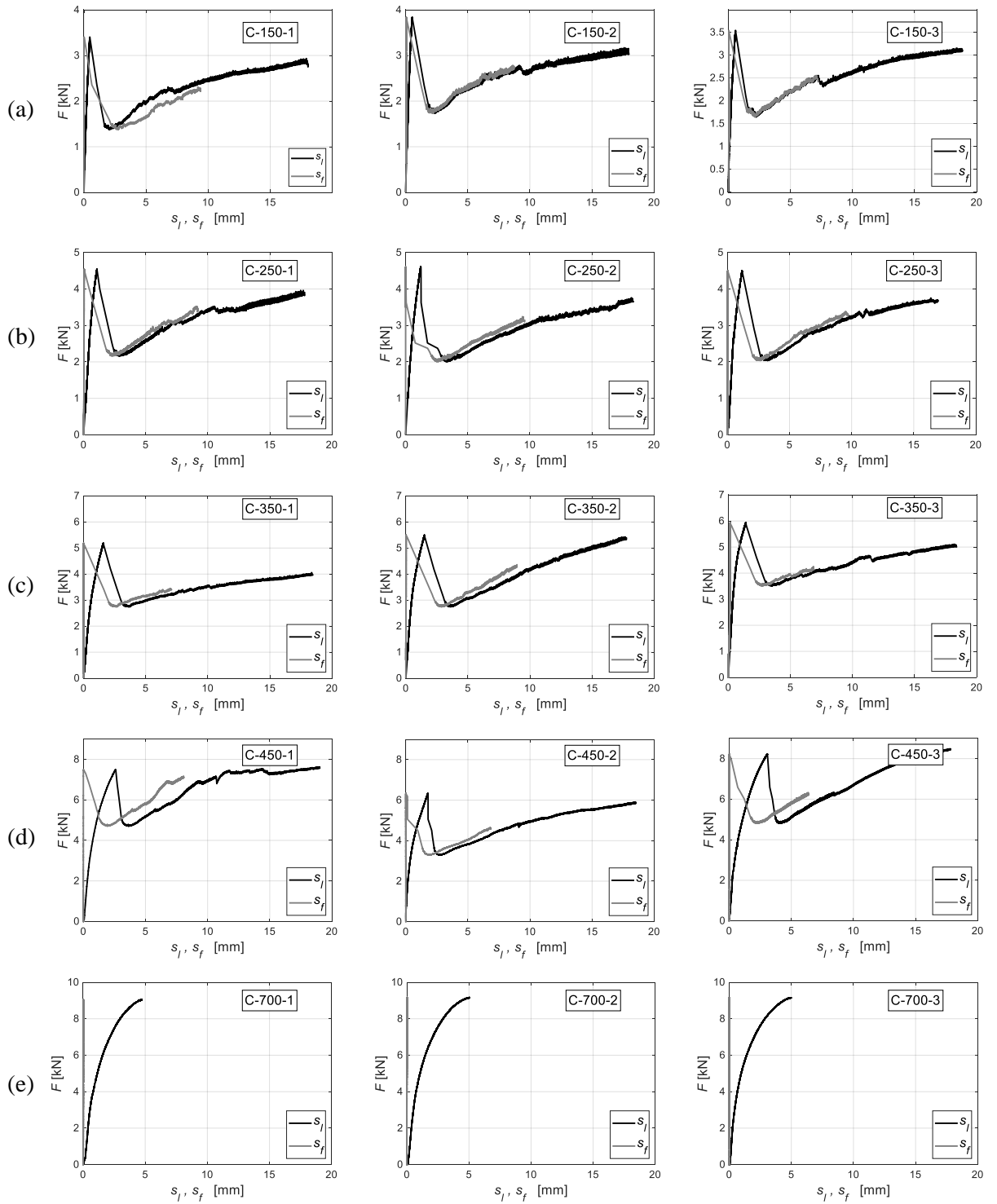| Bonded length, L_B [mm]	Cylindrical specimen name	F_m [kN]	$\bar{F}_m$ [kN] (CoV) [%]	s_{ml} [mm]	$\bar{s}_{ml}$ [mm] (CoV) [%]	Load drop, ΔF [kN]	Average load drop, $\Delta\bar{F}$ [kN] (CoV) [%]
150	C-150-1	3.40	3.59 (6.2)	0.49	0.53 (7.9)	2.01	1.96 (4.1)
	C-150-2	3.84		0.53		2.01	
	C-150-3	3.54		0.57		1.87	
250	C-250-1	4.54	4.55 (1.2)	1.28	1.23 (4.1)	2.33	2.32 (11.8)
	C-250-2	4.61		1.22		2.58	
	C-250-3	4.50		1.19		2.04	
350	C-350-1	5.19	5.54 (6.8)	1.58	1.49 (6.3)	2.45	2.54 (7.2)
	C-350-2	5.50		1.50		2.75	
	C-350-3	5.94		1.40		2.42	
450	C-450-1	7.50	7.35 (13.1)	2.59	2.48 (26.7)	2.81	3.08 (10.0)
	C-450-2	6.32		1.77		3.01	
	C-450-3	8.23		3.07		3.42	
700	C-700-1	9.05	9.12 (0.7)	4.73	4.92 (3.4)	/	/
	C-700-2	9.16		5.05		/	
	C-700-3	9.15		4.97		/	

4. RESULTS OF THE PULL-OUT TESTS FOR THE MASONRY SPECIMENS

Two main different failure modes were observed during the tests on the masonry wallettes and are reported in Figure 13. In 8 tests, the mortar joint, where the bar was embedded, detached from the bricks as the bar was pulled out (Type A in Figure 13), which resulted in the splitting of the masonry wallette. The detachment of the mortar_s from the bricks occurred at the actual interfacial surface between mortar and brick with no mortar left attached to the brick. For those 8 specimens, it was not possible to test the second bar. Pull-out of the bar without detachment of the mortar joints occurred in the remaining 11 specimens (Type B in Figure 13). However, it should be noted that fracture of the mortar in the transversal direction near the loaded end (regardless of whether the mortar joint detached from the brick) was observed in 13 tests. This additional phenomenon was accounted for by adding an asterisk next to the failure mode, i.e. A* or B* depending on whether it occurred prior to failure A or B. Figure 13 reports, as an example, a B* failure. Only in two cases, the splitting of the specimen occurred with transversal fracture of the mortar (A* failure mode) at the loaded end. The bonded length seems to have small influence on the failure mode of the specimens, since failures A, A*, B, and B* were observed for both short and long bonded lengths and a no clear trend could be pointed out,

although it should be noted that failure modes B and B* occurred more frequently for the longest bonded lengths.

Results of the tests on the bars embedded in masonry specimens are collected in Figures 14a-14e. In black, the F - s_l curves and in grey, the F - s_f curves, both reported in the same figure for bars with the same bonded length. The F - s_l curves show a trend similar to that reported for the cylindrical specimens and are characterized by three main branches: 1) an initial linear part for low load values followed by a non-linear part until the peak load is attained. The free-end slip values corresponding to this branch are very small and increase as the peak load is reached; 2) the peak load is followed by a load drop associated with an increase of the slip; and 3) an ascending almost-linear branch until the end of the test. As for the cylinders, the phenomenon of bar rotation about its longitudinal axis was visible during the tests on the wallettes.

Results for bars with L_B equal to 450 and 550 mm, Figures 14d and 14e, respectively, show that the slip at the free end is very small before the peak load at the end of the first branch is attained, which suggests that the effective bonded length is close to these length values. It can be noted that in some cases, F - s_f curves show some variability in the initial branch before the peak load is attained, i.e. s_f is greater than s_l, as in the case of specimen W-350-2B in Figure 14c. This behaviour can be due to the measurement system of the slip at the free end adopted in the case of masonry specimens. In fact, s_f is measured only by a single LVDT that reacted off of a circular plate attached to the free end of the bar. As stated before, during the test the bar rotates and the plate can be in some cases not perfectly horizontal, and this may result in a less reliable measurement of the free end slip.

The pull-out peak load F_m of the first branch and corresponding slip s_{ml} at the loaded end, as well as the corresponding average values ($\bar{F}_m$ and $\bar{s}_{ml}$), are reported for all the masonry specimens herein presented in Table 2. As for the cylindrical specimens, the pull-out load increases as the bonded length increases, and similar trend applies to the slip at the loaded end at peak. However, results show high coefficients of variation, especially for the loaded end slip. It is possible that the displacement measurement system at both loaded and free ends might be responsible in part for the variability of the results. Nevertheless, it should be taken into account that some variability is also inherently associated with the properties of the mortar especially when cast in small joints [19]. Interestingly, for some specimens (both mortar cylinders and

masonry wallettes) the load at the end of the third branch is higher than the first peak load F_m, which highlights the non-negligible residual load-carrying capacity due to the rotation of the bar. In Table 2, the load drop ΔF for each specimen and the average value $\Delta \overline{F}$ for each group are listed. It should be noted that for some specimens (in particular, W-150-4A, W-350-1A, W-450-4A, W-550-3A and W-550-4A) the value of ΔF is not reported since these specimens split apart at the mortar/brick interface (failure mode A or A*) soon after the first peak load was attained and, as a consequence, the load drop could not be measured. While for the remaining specimens that showed failure mode A or A* (in particular, W-150-1A, W-150-2A and W-150-3B), the load drop value is reported in Table 2 because the splitting at the brick/mortar interface occurred at the end of the ascending branch.

In Figure 14, considering F - s_l curves related to the specimens where both bar A and B were tested, i.e. W-150-3, W-250-1, W-250-3, W-350-2, W-450-2, W-450-3 and W-550-2, it could be noted that in some cases, curves are very close to each other (in particular, W-350-2A and B, W-450-2A and B, W-550-2A and B) and in other cases (in particular, W-150-3A and B, W-250-3A and B) bar B, which was tested after bar A, shows a better performance in terms of peak load F_m than bar A, envisaging that a bond degradation due to the previous testing of bar A was not present. In the remaining cases (in particular, W-250-1A and B, W-450-3A and B), curves related to bar A are higher than curves related to bar B. From these observations, the aspect of the possible interaction between two bars in the same specimens remains an open issue. Differences between two curves related to the same specimen may be also related to the inherent variability of the masonry and not because they interact. Additionally, since only 7 wallettes (out of 20) could be tested for both the bars, thus the possible interaction between two bars in a specimen still has to be confirmed by experimental evidence. In the light of the above-mentioned considerations, the fact that some specimens split apart when tested bar A, is a phenomenon more related to the problem of a poor brick/mortar adhesion than an interaction between bars.

| Failure mode A: splitting of the masonry wallette | Failure mode B: bar pull-out | Failure mode B*: bar pull-out with local fracture of the mortar |

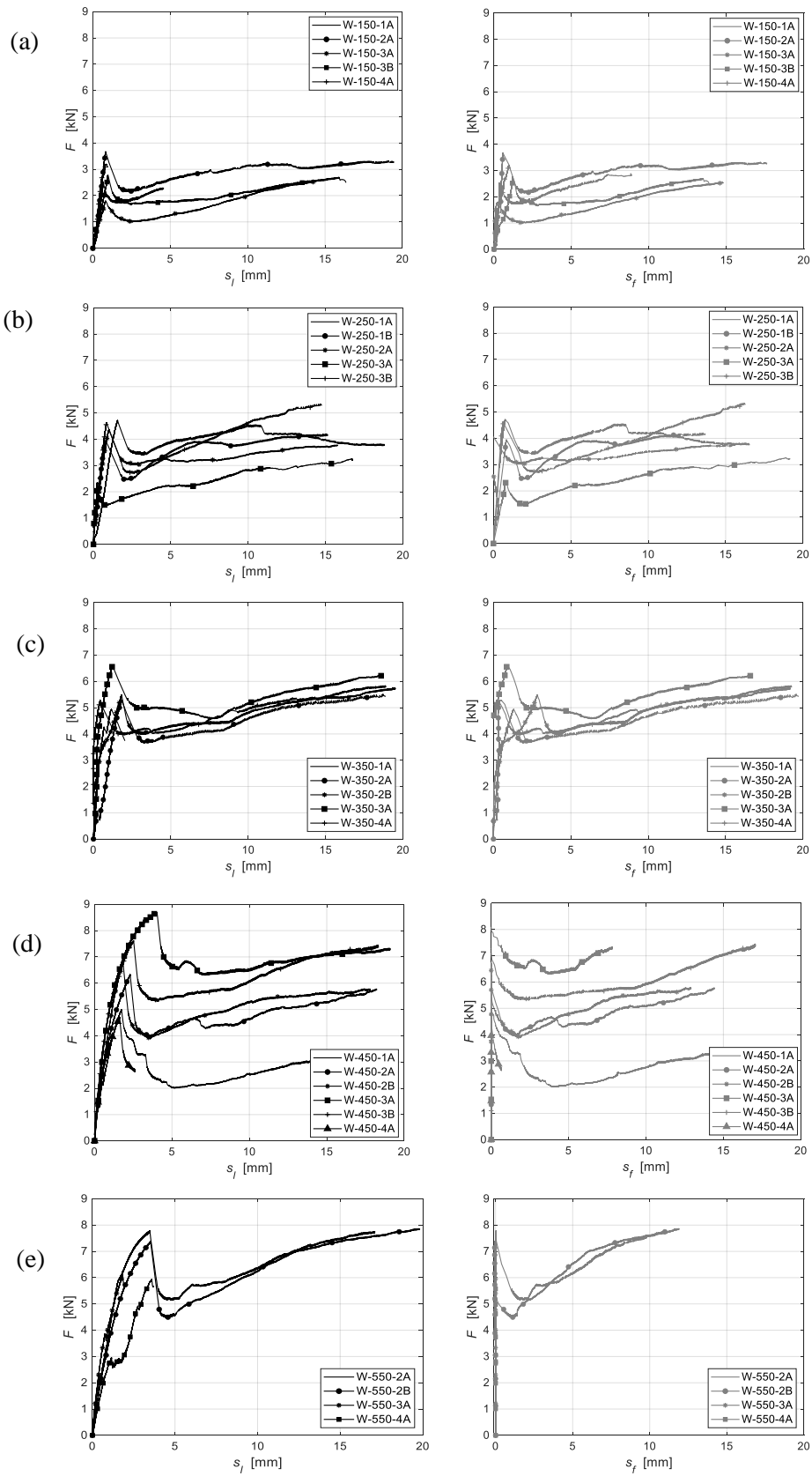Figure 13. Failure modes of the masonry specimens.

Figure 14. F - s_l (on the left column) and F - s_f (on the right column) curves for all masonry specimens. In each row, curves for specimens with the same bonded length are collected: a) W-150; b) W-250; c) W-350; d) W-450, and e) W-550.

Table 2. Pull-out test results for masonry specimens (coefficient of variation, CoV, in percentage within parentheses).

Bonded length, L_B [mm]	Masonry specimen label	Bar label	Failure mode	F_m [kN]	$\bar{F}_m$ [kN] (CoV) [%]	s_{ml} [mm]	$\bar{s}_{ml}$ [mm] (CoV) [%]	Load drop, ΔF [kN]	Average load drop, $\Delta\bar{F}$ [kN] (CoV) [%]
150	W-150-1	W-150-1A	A	2.52	2.79 (25.5) 2.69[1] (29.0)[1]	0.66	0.83 (13.6)	0.80	1.06 (33.1)
		W-150-1B	/	/		/		/	
	W-150-2	W-150-2A	A*	3.67		0.83		1.53	
		W-150-2B	/	/		/		/	
	W-150-3	W-150-3A	B*	1.79		0.82		0.78	
		W-150-3B	A	2.77		0.97		1.12	
	W-150-4	W-150-4A	A	3.20		0.87		/	
		W-150-4B	/	/		/		/	
250	W-250-1	W-250-1A	B*	4.71	4.00 (24.4) 4.00[1] (24.4)[1]	1.56	0.90 (51.3)	1.31	1.39 (27.1)
		W-250-1B	B*	3.94		0.79		1.49	
	W-250-2	W-250-2A	B*	4.37		1.01		1.33	
		W-250-2B	/	/		/		/	
	W-250-3	W-250-3A	B*	2.34		0.28		0.88	
		W-250-3B	B	4.64		0.84		1.92	
	W-250-4	W-250-4A	/	/		/		/	
		W-250-4B	/	/		/		/	
350	W-350-1	W-350-1A	A*	4.93	5.52 (11.6) 5.67[1] (11.2)[1]	1.15	1.29 (44.7)	/	1.53 (10.2)
		W-350-1B	/	/		/		/	
	W-350-2	W-350-2A	B*	5.29		1.82		3.66	
		W-350-2B	B*	5.49		1.82		3.98	
	W-350-3	W-350-3A	B*	6.61		1.24		4.94	
		W-350-3B	/	/		/		/	
	W-350-4	W-350-4A	B*	5.29		0.43		3.97	
		W-350-4B	/	/		/		/	
450	W-450-1	W-450-1A	B*	4.98	6.51 (23.4) 6.87[1] (20.2)[1]	1.74	2.34 (38.4)	2.98	2.58 (11.8)
		W-450-1B	/	/		/		/	
	W-450-2	W-450-2A	B	6.34		2.30		2.39	
		W-450-2B	B*	6.72		1.85		2.84	
	W-450-3	W-450-3A	B	8.68		4.04		2.38	
		W-450-3B	B	7.63		2.52		2.32	
	W-450-4	W-450-4A	A	4.71		1.62		/	
		W-450-4B	/	/		/		/	
550	W-550-1	W-550-1A	/	/	6.78 (13.8) 7.58[1] (3.9)[1]	/	3.10 (27.5)	/	2.76 (6.6)
		W-550-1B	/	/		/		/	
	W-550-2	W-550-2A	B	7.79		3.47		5.16	
		W-550-2B	B	7.37		3.53		4.48	
	W-550-3	W-550-3A	A	6.04		1.82		/	
		W-550-3B	/	/		/		/	
	W-550-4	W-550-4A	A	5.93		3.59		/	
		W-550-4B	/	/		/		/	

[1] $\bar{F}_m$ average values and CoV in percentage within parentheses computed without considering specimens that exhibited splitting as soon as the first peak load was attained

26

5. COMPARISON BETWEEN CYLINDRICAL AND MASONRY SPECIMENS

In Figure 15a, the average pull-out load $\overline{F}_m$ for both cylindrical and masonry specimens with the same bonded length is plotted versus the bonded length L_B itself. It should be noted that the value of $\overline{F}_m$ for masonry specimens were computed without considering the specimens that exhibited splitting as soon as the first peak load was attained. Removing those specimens from the calculation of the average was necessary to consider the trend of consistent wallettes with the same type of failure, Table 2. As the bonded length increases, the pull-out load increases non-linearly while approaching the tensile limit of the bar. It is worth noting that the average peak load of cylinders differs than the one of masonry specimens by 33%, 14%, -2% and 7% for L_B equal 150, 250, 350 and 450 mm, respectively. Those differences are not negligible for some bonded lengths, but they should be interpreted in the context of the values of CoV for the peak load of masonry specimens, which are as high as 29% for L_B equal 150 mm. The differences in peak load between cylindrical and masonry specimens can also in part be attributed to the different confining role of the material surrounding the bar. In the cylinders, the mortar is able to provide a homogenous confining action, while in masonry specimens the weak plane at the mortar-brick interface might influence the confining action of the surrounding material. It should be mentioned that the properties of the mortar cast in large cylindrical specimens might be different from the properties of the mortar cast in a thin joint [29]. In addition, the eccentric position of the masonry specimens with respect to the load axis might have played a role in the bond behavior of the bar. The results indicate that testing cylindrical specimens might provide an upper bound of the bond behavior of the bars in actual masonry applications. It should be pointed out that additional tests on masonry specimens should be carried out in which a transversal compression on the masonry wallette is applied. The trend of Fig. 15a indicates that for both cylindrical specimens and masonry wallettes the effective bond length is greater than the bonded lengths tested. However, to confirm this trend, additional lengths should be considered.

Figure 15b shows the average of the slip at the loaded-end corresponding to the peak load, $\overline{s}_{ml}$, plotted versus the bonded length for cylinders and wallettes. The trend is very similar for the two types of specimens.

The average load drop, $\Delta\overline{F}$, is calculated as the average of the difference between the peak load and the load corresponding to the relative minimum after the drop for each specimen (Table 2). It could be seen in Figure

15c that $\Delta\bar{F}$ is increasing with increasing L_B. One possible explanation for the trend of $\Delta\bar{F}$ is that as the peak is reached, damage has occurred along the entire bonded length. Since the tests were run in LVDT stroke control, a load decrease is necessary after the peak to increment the controlling displacement. The load reaches a relative minimum after the peak that is associated with the condition of the surrounding mortar. In longer bonded lengths, the mortar close to the loaded end is further damaged prior to reaching the peak as the damage progresses along the bar. Thus, the increased damage of the mortar for longer bonded lengths could be responsible for the trend observed in Figure 15c. In other words, a more substantial damage of the mortar corresponds to less resistance as the bar tends to slip after the bond has been compromised.

In order to compare applied load versus loaded end slip curves for cylinders and masonry, one representative curve per bonded length for cylinders and masonry specimens is plotted in Figures 16a and 16b, respectively, where curves with the same color correspond to the same bonded length. It should be noted that in Figures 16a and 16b, only a curve per specimen type is reported, since the first branch overlaps both for cylinders and masonry wallettes with the same bonded length. As expected, a greater variability can be envisaged in the slope of the first branch for the masonry wallettes (see Figure 14, black curves) with respect to the cylinder results, however the fluctuations can be considered acceptable for this kind of specimens. Additionally, to realize Fig. 16b, only a curve with an average behaviour was selected since it was considered more representative of the average behaviour for that specific bond length.

The initial stiffness of the F - s_l curves appears to be similar for specimens of the same type and different bonded lengths, which is an indication of the consistency of the results and the reliability of the test set-up. The curves tend to be non-linear close to the peak and the non-linearity is more evident as L_B increases. To further strengthen the comment above related to the trend of $\Delta\bar{F}$, it should be noted that after the relative minimum is reached, the last increasing branch appears to be linear with a slope that is consistent among the different bonded lengths. However, for both cylinders and wallettes, the last portion of the third branch is non-linear for the longest bonded length, related to the high degree of damage that accumulates along the bar as the peak is reached in the longest bars.

It should also be noted that in literature the bond between reinforcing bars and concrete as well as between fiber-reinforced polymer (FRP) composites and a substrate are typically described as Mode-II fracture

mechanics problem [36, 37]. Shear stresses develop along the bonded length that are associated with slip between the two adherents. As the load applied to the bar or composite increases, the shear stress distribution along the bonded length evolves. As the bonded length increases, the load required to have shear stresses distributed over the entire bonded length increases as well. The maximum load might not be attained when the full shear stress distribution is first reached if friction/interlocking phenomena occur. In addition, the relationship between the peak load and the bonded length might not be linear as these interfacial problems are typically described by a cohesive material law (shear stress versus slip) that exhibits a softening branch. If slips at the free-end are observed for values of the applied load that are substantially smaller than the maximum load it is possible that: 1) the bonded length is not sufficient to full establish the shear stress distribution; and/or 2) the friction/interlocking is a major contribution in the adhesion of the materials investigated. The results herein provided are discussed taking into account these general observations for interfacial problems.
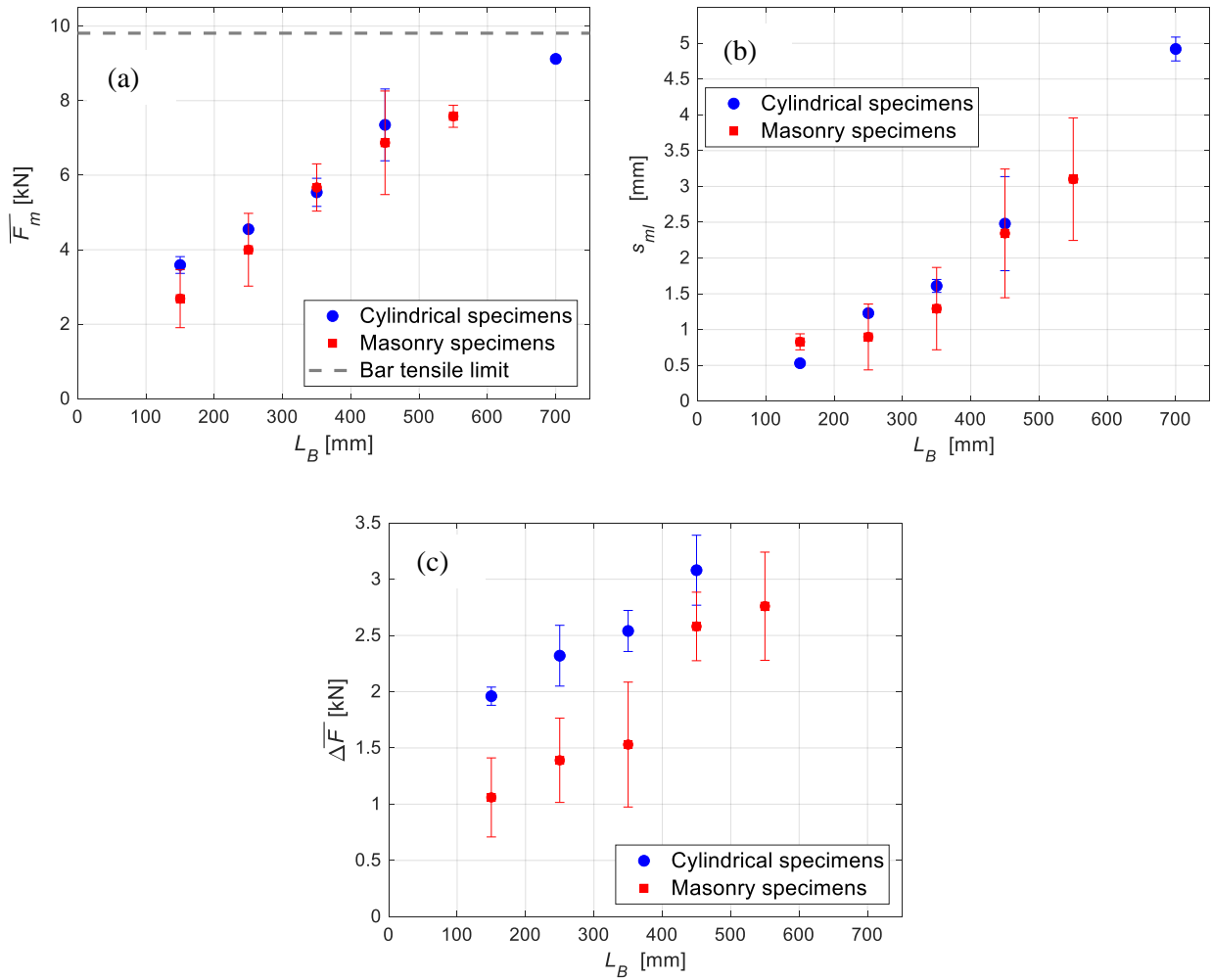
Figure 15. Relationship between (a) $\overline{F_m}$ and L_B, (b) $\overline{s}_{ml}$ and L_B and (c) $\Delta\overline{F}$ and L_B for cylindrical and masonry specimens with error bars.
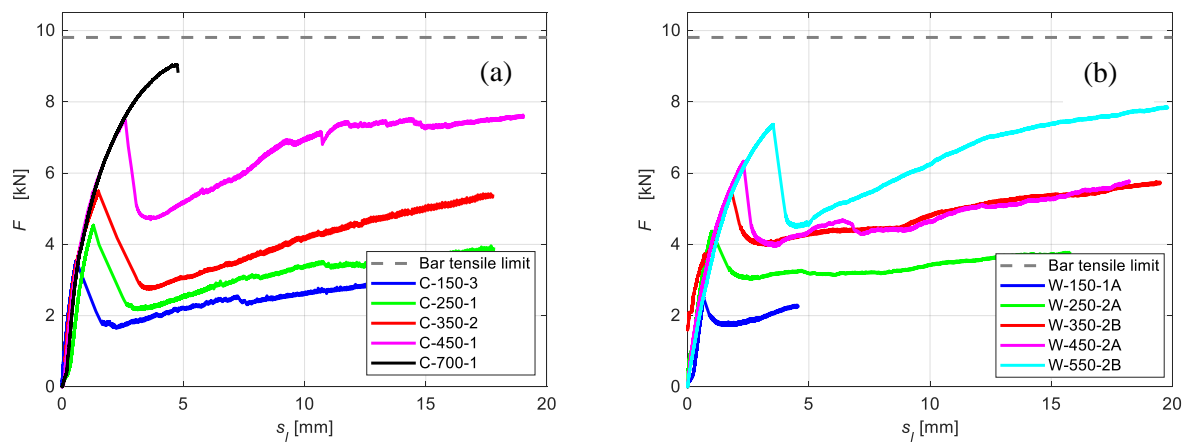

Figure 16. F - s_l curves of representative a) cylindrical and b) masonry specimens for different bonded lengths.

6. CONCLUSIONS

This paper presented an investigation on the pull-out behavior of high-strength twisted steel bars that are commonly employed as reinforcing material in structural repointing applications on masonry structures. Two experimental programs were conducted: in the first one, the bars were embedded concentrically in cylinders made of structural mortar, and in the second one the bars were inserted (using the same mortar the cylinders were made of) few centimetres from the outer surface of masonry wallettes, to replicate the in-situ applications. In both experimental campaigns, the bars were pulled while the cylinder or the masonry wallette were restrained. One of the key objectives of the experimental work was the study of the effect of the bonded length on the pull-out behavior of the bars. In order to compare the results, the same bonded lengths were considered both in the cylinders and masonry specimens. To the authors' knowledge, the literature available on the study of the pull-out behaviour of such bars inserted in the bed joints of masonry wallettes is extremely limited and this study is intended to give a preliminary contribution to the field.

From the experimental results, the following conclusions can be drawn:

1. both masonry and mortar cylindrical specimens exhibited a similar load versus loaded-end slip response, characterized by three branches. In the first branch, the load response was pseudo-linear for low load values and then non-linear up to the peak. The second branch was associated with a drop on the load and increase of the loaded-end slip. Finally, in the third branch the load increased almost linearly;

2. for all cylindrical specimens, the bars slipped with respect to the cylinder until the test was stopped, except for the bars with a bonded length equal to 700 mm that failed in tension. The average peak load increased almost linearly with the bonded length L_B, which indicates that the effective bond length could not be reached prior to the failure of the bar in tension;

3. for masonry specimens, the majority of the bars slipped with respect to the masonry wallette until the test was stopped. For seven specimens, splitting of the masonry specimens occurred, which appeared to be associated with a lower peak load with respect to those specimens for which slippage occurred without splitting. In both failure modes, transversal cracks in the mortar near the loaded end were observed for some specimens;

4. for masonry specimens, it was shown that the peak load increased with an increase in the bonded length. However, it should be noted that the trend might be deceiving for the longest bonded length, since two specimens out of four for that length exhibited splitting of the masonry wallette along the joint where the bar was inserted. Longer bonded lengths should be considered to confirm this result. It is possible that longer masonry wallettes might split without the use of a transversal compression;

5. for masonry and cylindrical mortar specimens, as the bar slipped, rotation of the bar itself was observed due to its shape. After the attainment of the peak pull-out load at the end of the first branch, the bar showed additional load-carrying capacity due not only to friction between the bar and the surrounding mortar, but also to the presence of the mortar between the ribs.

It is important to recognize that these bars are characterized by a complex behaviour that produces a high variability in the test outcomes, in particular in the case of masonry specimens, thus it is recommended that further research is conducted to confirm the results herein presented and to expand the database on the topic.

REFERENCES

[1] Corradi, M., Borri, A. A database of the structural behavior of masonry in shear. Bulletin of Earthquake Engineering, 16, 3905-3930 (2018).

[2] Franzoni, E., Gentilini, C., Santandrea, M., Zanotto, S., Carloni, C. Durability of steel FRCM-masonry joints: effect of water and salt crystallization. Materials and Structures/Materiaux et Constructions, 50 (4), art. no. 201 (2017).

[3] Castellazzi, G., D'Altri, A.M., de Miranda, S., Ubertini, F. An innovative numerical modeling strategy for the structural analysis of historical monumental buildings. Engineering Structures, 132, 229-248 (2017).

[4] Hofer, L., Zampieri, P., Zanini, M.A., Faleschini, F., Pellegrino, C. Seismic damage survey and empirical fragility curves for churches after the August 24, 2016 Central Italy earthquake. Soil Dynamics and Earthquake Engineering, 111, 98-109 (2018).

[5] Sorrentino, L., Cattari, S., da Porto, F., Magenes, G., Penna, A. Seismic behaviour of ordinary masonry buildings during the 2016 central Italy earthquakes. Bulletin of Earthquake Engineering, 17, 5583–5607 (2019).

[6] Fiorentino, G., Forte, A., Pagano, E., Sabetta, F., Baggio, C., Lavorato, D., Nuti, C., Santini, S. Damage patterns in the town of Amatrice after August 24th 2016 Central Italy earthquakes. Bulletin of Earthquake Engineering, 16, 1399-1423 (2018).

[7] Crespi P., Franchi A., Giordano N., Scamardo M., Ronca P. Structural analysis of stone masonry columns of the Basilica S. Maria di Collemaggio. Engineering Structures, 129, 81-90 (2016).

[8] Indirli, M., Kouris, L.A.S., Formisano, A., Borg, R.P., Mazzolani, F.M. Seismic damage assessment of unreinforced masonry structures after the Abruzzo 2009 earthquake: The case study of the historical centers of L'Aquila and Castelvecchio Subequo. International Journal of Architectural Heritage, 7, 536-578 (2013).

[9] Valluzzi, M.R., Binda, L., Modena, C. Mechanical behaviour of historic masonry structures strengthened by bed joints structural repointing. Construction and Building Materials, 19, 63–73 (2005).

[10] Borri, A., Castori, G., Corradi, M. Behavior of masonry columns repaired using small diameter cords. Key Engineering Materials, 624, 254–265 (2015).

[11] Casacci, S., Di Tommaso, A., Gentilini, C. Crack propagation in compression and mounted arrestors. Key Engineering Materials, 624, 595-602 (2015).

[12] Maragna, M., Casacci, S., Gentilini, C. In-plane shear behaviour of masonry wall panels strengthened by structural repointing. International Journal of Masonry Research and Innovation, 1 (3), 253-276 (2016).

[13] Casacci, S., Gentilini, C., Di Tommaso, A., Oliveira, D.V. Shear strengthening of masonry wallettes resorting to structural repointing and FRCM composites. Construction and Building Materials, 206, 19-34 (2019).

[14] Akhaveissy, A.H., Milani, G. A numerical model for the analysis of masonry walls in-plane loaded and strengthened with steel bars. International Journal of Mechanical Sciences, 72, 13–27 (2013).

[15] Garbin, E., Valluzzi, M.R., Modena, C. Testing and numerical modelling of the structural behaviour of brick masonry strengthened by the bed joints reinforcement technique. 1st WTA - International PhD Symposium - Building Materials and Building Technology for Preservation of the Built Heritage (2009).

[16] Petersen, R.B., Masia, M.J., Seracino, R. Bond behavior of near-surface mounted FRP strips bonded to modern clay brick masonry prisms: influence of strip orientation and compression perpendicular to the strip. Journal of Composites for Constructions, 13, 169-178 (2009).

[17] Moreira, S., Ramos, L.F., Csikai, B., Bastos, P. Bond behaviour of twisted stainless steel bars in mortar joints. 9th International Masonry Conference, Guimarães (2014).

[18]   Osofero, A.I., Corradi, M., Borri, A. Experimental study of bond strength between titanium bar and lime-based mortar. Journal of Materials in Civil Engineering, 27, 04014182-1,10 (2015).

[19]   Maljaee, H., Ghiassi, B., Lourenço, P.B. Bond behavior in NSM-strengthened masonry. Engineering Structures, 166, 302–313 (2018).

[20]   Gentilini, C., Finelli, F., Girelli, V.A., Franzoni, E. Pull-out behavior of twisted steel connectors employed in masonry: The influence of the substrate. Construction and Building Materials, 274, art. no. 122115, (2021).

[21]   De Lorenzis, L., and A. Nanni. Bond between near-surface mounted fiber-reinforced polymer rods and concrete in structural strengthening. ACI Structural Journal, 99, 123–132 (2002).

[22]   Turco, V., Secondin, S., Morbin, A., Valluzzi, M.R., Modena, C. Flexural and shear strengthening of un-reinforced masonry with FRP bars. Composites Science and Technology, 66, 289-296 (2006).

[23]   Willis, C.R., Yang, Q., Seracino, R., Griffith, M.C. Bond behaviour of FRP-to-clay brick masonry joints. Engineering Structures, 31, 2580-2587 (2009).

[24]   Kashyap, J., Willis, C.R., Griffith, M.C., Ingham, J., Masia, M.J. Debonding resistance of FRP-to-clay brick masonry joints. Engineering Structures, 41, 186-198 (2012).

[25]   Dizhur, D., Griffith, M.C., Ingham, J.M. Pullout strength of NSM CFRP strips bonded to vintage clay brick masonry (2014) Engineering Structures, 69, pp. 25-36.

[26]   Li, T., Galati, N., Tumialan, J.G., Nanni, A. Analysis of unreinforced masonry concrete walls strengthened with glass fiber-reinforced polymer bars. ACI Structural Journal, 102 (4), 569-577 (2005).

[27]   Yu, P., Silva, P., Nanni, A. In-plane Performance of unreinforced concrete masonry strengthened with prestressed GFRP bars. Journal of Composites for Constructions, 21, art. no. 04016064 (2017).

[28]   EN 998-2. Specification for mortar for masonry. Part 2: Masonry mortar (2016).

[29]   Franzoni, E., Gentilini, C., Santandrea, M. et al. Durability of steel FRCM-masonry joints: effect of water and salt crystallization, Materials and Structures 50, 201 (2017).

[30]   EN 1015-11. Methods of test for mortar for masonry. Part 11: Determination of flexural and compressive strength of hardened mortar (2001).

[31]   EN 12390-13. Testing hardened concrete. Determination of secant modulus of elasticity in compression (2013).

[32]   EN 772–1. Methods of test for masonry units. Part 1: Determination of compressive strength (2015).

[33]   Karmokar, T., Mohyeddin, A., Lee, J., Paraskeva, T. Concrete cone failure of single cast-in anchors under tensile loading – A literature review, Engineering Structures, 243, 112615 (2021).

[34]   Węglorz, M. Influence of headed anchor group layout on concrete failure in tension, Procedia Engineering, 193, 242-249 (2017).

[35]   ASTM D7913 / D7913M – 14. Standard test method for bond strength of fiber-reinforced polymer matrix composite bars to concrete by pullout testing (2020).

34

[36]   Focacci, F., Nanni, A., Bakis, C.E. Local bond-slip relationship for FRP reinforcement in Concrete. Journal of Composites for Construction, 4, 24–31 (2000).

[37]   Focacci, F., D'Antino, T., Carloni, C., Sneed, L.H., Pellegrino, C. An indirect method to calibrate the interfacial cohesive material law for FRCM-concrete joints. Materials and Design, 128, 206–217, (2017).

1
2
3
4
5
6
7
8
9
10
11
12
13
14
15
16
17
18
19
20
21
22
23
24
25
26
27
28
29
30
31
32
33
34
35
36
37
38
39
40
41
42
43
44
45
46
47
48
49
50
51
52
53
54
55
56
57
58
59
60
61
62
63
64
65

35